Department of Physics and Astronomy
Heidelberg University

Bachelor Thesis in Physics
submitted by

Hjalmar Brunßen

born in Frankfurt am Main (Germany)

2022

Hydrodynamic modeling of J/ψ transverse momentum spectra and anisotropic flow at $\sqrt{s_{\mathrm{NN}}} = 5.02$ TeV using Fluid$u$M

This Bachelor Thesis has been carried out by Hjalmar Brunßen at the
Physikalisches Institut in Heidelberg
under the supervision of
Prof. Dr. Johanna Stachel

Abstract

In ALICE, relativistic heavy-ion collisions are studied in order to gain an understanding of the quark-gluon plasma. This thesis is intended to approach this from a phenomenological perspective by the study of transverse momentum spectra and the anisotropic flow. With Fluid$u$M, a hydrodynamic modeling of the quark-gluon plasma is implemented with a very high numerical efficiency, which is attributed to a background-perturbation splitting of the fluid dynamic fields and a mode expansion of the perturbation fields. Starting from a previous parameter optimization of transverse momentum spectra of light flavor hadrons (namely pions, kaons and protons) for Pb-Pb collisions at $\sqrt{s_{\mathrm{NN}}} = 2.76\,\mathrm{TeV}$, the modeling of the same observable is performed for $\sqrt{s_{\mathrm{NN}}} = 5.02\,\mathrm{TeV}$. Based on this altogether reasonable model description of the thermalized production of light flavor hadrons, the Fluid$u$M framework is used for the determination of J/ψ transverse momentum spectra and elliptic as well as triangular flow. In order to account for the charm enhancement, this is done using predictions of the statistical hadronization model. The corresponding results are compared to experimental data and predictions from the alternative hydrodynamic model MUSIC.

Zusammenfassung

In ALICE werden relativistische Schwerionenkollisionen untersucht, um ein tieferes Verständnis des Quark-Gluon-Plasmas zu erlangen. Diese Arbeit versucht sich diesem Ziel von einer phänomenologischen Perspektive zuzuwenden, indem die Transversalimpuls-Spektren und der anisotrope Flow untersucht werden. Ausgehend von einer vorherigen Parameteroptimierung für die Transversalimpuls-Spektren bei $\sqrt{s_{\mathrm{NN}}} = 2.76\,\mathrm{TeV}$ von Hadronen leichten Flavors (nämlich Pionen, Kaonen und Protonen), wird dieselbe Observable für $\sqrt{s_{\mathrm{NN}}} = 5.02\,\mathrm{TeV}$ modelliert. Basierend auf der ingesamt sinnvollen Beschreibung der thermalisierten Erzeugung von Hadronen leichten Flavors durch das Modell, wird Fluid$u$M für die Bestimmung der Transversalimpuls-Spektren sowie des elliptischen und dreieckigen Flows des J/ψ verwendet. Um das Charm-Enhancement zu berücksichtigen werden Konzepte des Modells der statistischen Hadronisierung (SHM) verwendet. Die entsprechenden Vorhersagen werden mit den experimentellen Daten sowie jenen eines anderen hydrodynamischen Modells - MUSIC - verglichen.

Contents

1. Introduction

1.1. Introduction to the Quark-Gluon Plasma

The matter that we face in our world is made of hadrons - color neutral objects consisting of quarks and gluons. This phenomenon, that quarks cannot occur individually at our typical energy and density scales is called confinement. It is a fundamental property of quantum chromodynamics (QCD) - the underlying quantum field theory of the strong interaction between quarks and gluons.
If one considers nuclear matter at high temperatures or densities, the asymptotic freedom causes a decrease of the strong interaction. Consequently, the quarks can cover distances that are much larger than the size of hadrons. This allows the existence of a phase of matter consisting of deconfined quarks and gluons, called quark-gluon plasma (QGP). There exists a phase transition between the confinement (hadronic matter) and the QGP region of the phase diagram sketched in figure 1.1. The transition at low baryon chemical potential is expected to happen as a continous crossover. This QGP is also expected to be formed in the early universe within the first 10 microseconds after the Big Bang due to its high temperature and density [1, 2].

Experimentally, we can reach sufficiently high temperatures in relativistic heavy-ion collisions. The QGP produced in these collisions cools down very rapidly (10^{-23} s) until a critical temperature is reached where confinement holds so that hadrons are formed out of the quarks in the medium. This has been studied in the Super Proton Synchrotron (SPS), Relativistic Heavy Ion Collider (RHIC), Alternating Gradient Synchrotron (AGS) and the Large Hadron Collider (LHC) in the last decades [4].
These studies offer unique prospects to gain a deeper insight into the properties of the QGP, the nature of (de-)confinement and the corresponding phase transition. Moreover, the realization of QCD in a relativistic quantum fluid and the possibility to test predictions of QCD arouses interest from theoretical as well as experimental perspectives.

This thesis will do a study of transverse momentum spectra and anisotropic flow at LHC

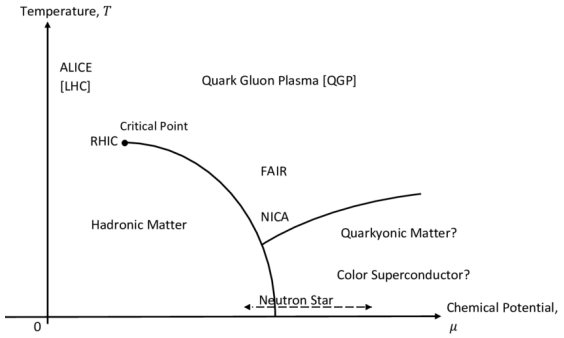

Figure 1.1.: QCD phase diagram showing the temperature against the baryochemical potential. Taken from [3] (CC-BY-4.0 license)

energies of $\sqrt{s_{\mathrm{NN}}} = 5.02\,\mathrm{TeV}$ based on a hydrodynamic modeling with Fluid$u$M. This chapter will start with a general introduction of some key concepts and quantities, that are crucial for the later analysis. Chapter 2 will concentrate on the ideas behind the hydrodynamical model Fluid$u$M and will also give an introduction into the statistical hadronization model, which will applied later-on. Chapter 3 will present the results from transverse momentum spectra and anisotropic flow analyses. It will begin with a comparison of these quantities for hadrons with the experimental data and will continue with the corresponding analysis for the J/ψ using the statistical hadronization model. The results and interpretations will be discussed in chapter 4.

1.2. Ultra-Relativistic Heavy-Ion collisions

In ultra-relativistic heavy-ion collisions, the collision takes place between two heavy nuclei – in the case of LHC lead (Pb) is used. The collisions are in general not head-on, but have an almond-shaped overlap zone as depicted in figure 1.2. Nucleons inside this overlap are called participants or (nearly synonymously for ultra-relativistic collisions) wounded nucleons if they undergo at least one inelastic scattering. Particles outside this overlap zone are called spectators. One defines the impact vector $\mathbf{b}$ as the vector in the plane perpendicular to the beam axis between the centers of both nuclei. The impact vector and the beamline span the reaction plane.

The impact parameter, which is the absolute value of the impact vector, cannot be directly observed in the experiment. For this reason, the initial shape of the collision is characterized in terms of centrality: it is the percentage of events that have a higher multiplicity [4]. The centrality is monotonically related to the impact parameter because

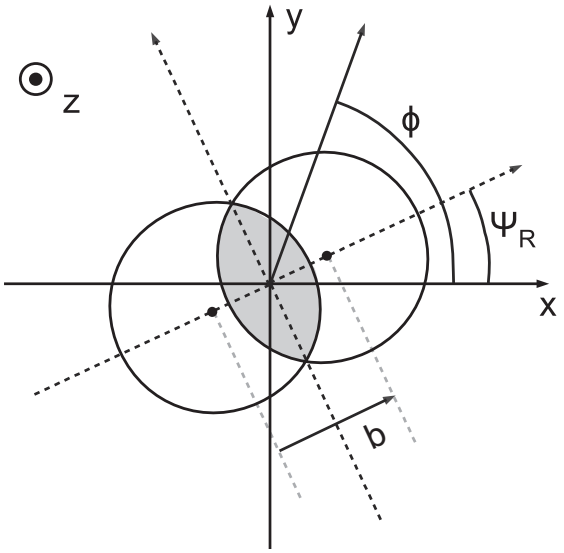

Figure 1.2.: Sketch of the collison geometry in the transverse plane of a heavy-ion collision. The impact vector **b** the reaction plane angle Ψ_R and the azimuthal angle ϕ are depicted. Taken from [5] (CC-BY-3.0 license)

a higher number of participant typically causes a higher multiplicity. With this definition, single events can be classified into centrality classes e.g., $0 - 5\%$ for the most central collisions.

1.3. Evolution of the Quark-Gluon Plasma

Immediately after the collision, an out-of-equilibrium evolution is initiated. After a very short time (of the order of $1\,\mathrm{fm}/c$), the medium of quarks and gluons reaches to a sufficient degree local thermal equilibrium. Its evolution can therefore be described by relativistic hydrodynamics [4]. The hot and dense medium, which is shown to constitute an almost ideal fluid [6], continues to cool down during its expansion.
When it reaches a sufficiently low temperature, the decoupling of hadrons takes place. This is called the freeze-out and is expected to happen in different stages. The kinetic or thermal freeze-out describes the transition to a stage where the interaction between the hadrons is very low. This can be related to a mean free path of the hadrons becoming similar to the system size. The chemical freeze-out takes place even earlier. It is based on the phenomenon that inelastic scatterings stop before the elastic scatterings when the system cools down [4]. The production of particles around the freeze-out temperatures is described by the Cooper-Frye formula, which will be explained in detail in section 2.3.

One of the early results of relativistic heavy-ion collisions is that the quark-gluon plasma can be described as a nearly perfect fluid [6]. It is characterized by the shear viscosity over entropy density η/s. In strongly coupled systems, a universal lower bound for η/s was proposed by Son based on the „AdS/CFT“ correspondence of anti-de Sitter space and conformal field theories [7]. The corresponding value of the universal lower bound is given by $(\eta/s)_{\mathrm{min}} = \hbar/(4\pi k_{\mathrm{B}}) \approx 0.08\,\hbar/k_{\mathrm{B}}$ with the reduced Planck constant $\hbar = h/(2\pi)$ and the Boltzmann constant k_{B}. The experimental evidence of the QGP produced in heavy-ion collisions is consistent with a η/s near this lower bound. Results from RHIC suggest a value $\eta/s < 0.24\,\hbar/k_{\mathrm{B}}$ corresponding to three times the lower bound [8]. The experimental value is a clear support for the picture of the QGP as a strongly-coupled nearly-perfect fluid.

1.4. Anisotropic Flow

The distribution of momenta in the transverse plane is obviously to some extent asymmetric. Even for the most central collisions, the overlap region is not entirely homogeneous but contains statistical fluctuations. In general, every heavy-ion collision possesses an anisotropy due to the its eccentricity (of the „almond shape“) as well as due to random fluctuations. Because of the pressure gradient, the initial anisotropy in real space induces also a non-trivial azimuthal dependence of the produced particles in momentum space. Consequently, it depends strongly on the transport properties such as η/s [11].

The azimuthal dependence of the transverse momentum is described by a Fourier decomposition of the azimuthal particle distribution [11] leading to:

$$E\frac{\mathrm{d}^3N}{\mathrm{d}\mathbf{p}^3} = \frac{\mathrm{d}^2N}{2\pi p_{\mathrm{T}}\,\mathrm{d}p_{\mathrm{T}}\,\mathrm{d}y}\left[1 + \sum_{n=1}^{\infty} 2v_n \cos(n(\phi - \Psi_n))\right] \tag{1.1}$$

ϕ indicates here the azimuthal angle, Ψ_n is the n-th harmonic symmetry plane defining the symmetry axis of the corresponding anisotropy and v_n denotes the anisotropic flow coefficients.

In the hypothetical case of no fluctuations and a corresponding momentum anisotropy being solely determined by the shape of the overlapping zone, Ψ_n would be the reaction plane angle (with respect to an event-independent x direction) and the Fourier

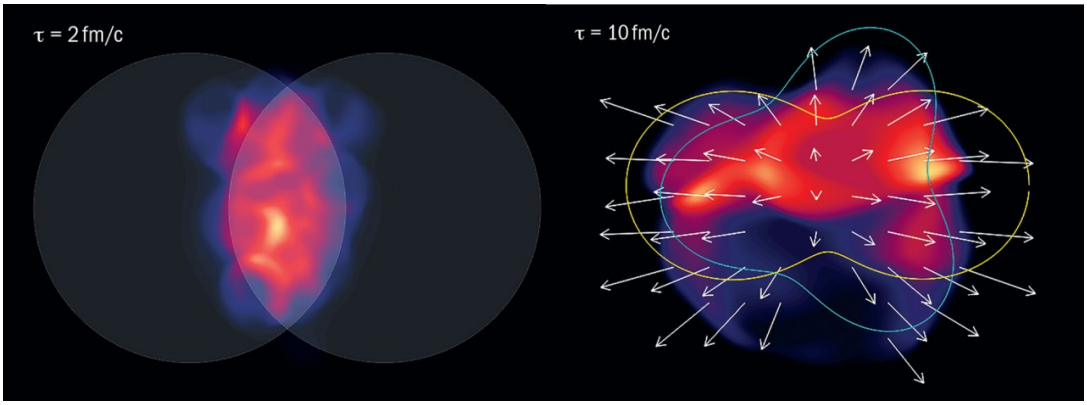

Figure 1.3.: Evolution of the quark gluon plasma obtained from a hydrodynamic simulation with MUSIC [9]. The evolution from an early time (left) to a late time (right) of the medium can be seen. On the right-hand side, the corresponding elliptic (yellow) and triangular (blue) flow is illustrated by the two colored shapes. Taken from [10].

coefficients would be given by [12]:

$$v_n(p_\mathrm{T}\,, y) = \langle \cos[n(\phi - \Psi_\mathrm{RP})] \rangle \tag{1.2}$$

For symmetry reasons, this would lead to non-vanishing terms only for even Fourier orders. Of course, this is not true for the general formula 1.1 and in this thesis, the resulting v_3 from the hydrodynamic evolution with Fluid$u$M will be studied.

The coefficients v_1, v_2 and v_3 are called the directed, elliptic and triangular flow, respectively. The latter two are sketched in figure 1.3. The elliptic flow v_2 is negative at low beam energies corresponding to more particles being emitted perpendicular to the reaction plane (out-of-plane flow) and positive (in-plane flow) at higher beam energies. This can be understood as an effect of spectators blocking the expansion in the reaction plane at low energies, whereas at high energies they pass sufficiently fast, so that the system can expand into the direction of the highest pressure gradient [4].

2. Modeling of the Quark-Gluon Plasma

„Fluid dynamics of heavy ion collisions with Mode expansion“ (Fluid$u$M) [13] is a framework written in mathematica, which calculates the viscous relativistic fluid dynamics of the QGP. In order to describe the physical system and the observables, initial conditions for the hydrodynamic evolution are needed and will be provided by the T$_\mathrm{R}$ENTo model [14] in this thesis. In addition, FastReso [15], a program calculating the contributions of resonance decays to the particle distributions, is applied. The combination of all three allows to make predictions about the produced particles after the hydrodynamic expansion and the freeze-out. This chapter is meant to give a general idea of the framework, but does not claim to give a complete description. For a more detailed explanation and derivation, the paper from S. Floerchinger, E. Grossi and J. Lion [13] should serve as a main reference.

The Fluid$u$M code is mainly based on two concepts: a background-fluctuation splitting and a mode expansion for the fluid-dynamic evolution [13]. This allows to implement the hydrodynamic evolution in a numerically extremely efficient and still very accurate way.

2.1. Initial Conditions

The initial conditions for the hydrodynamic evolution in terms of an entropy density profile are computed from the „Reduced Thickness Event-by-event Nuclear Topology“ model (T$_\mathrm{R}$ENTo). It is a purely geometric approach that does not make assumptions about the physical processes behind the entropy production, non-equilibrium dynamics and thermalization [14]. The general assumption is the existence of a scalar field which is proportional to the entropy deposited in the central rapidity region at the initial proper

time τ_0. This is postulated to be fulfilled by the reduced thickness:

$$\left.\frac{\mathrm{d}S}{\mathrm{d}y}\right|_{\tau=\tau_0} \propto T_\mathrm{R}(p; T_A, T_B) = \left(\frac{T_A^p + T_B^p}{2}\right)^{1/p} \tag{2.1}$$

$T_i(x,y) = \int \rho_i^\mathrm{part}(x,y,z)\,\mathrm{d}z\,,\ i \in \{A,B\}$ is the thickness function of the colliding nuclei, ρ_i^part is the corresponding density of nuclear matter that participates in inelastic collisions and $p \in \{-\infty, \infty\}$ is a continuous, dimensionless parameter. The latter determines the combination of the individual thickness functions in a generalized mean: $p = 1, 0, -1$ correspond to the arithmetic, geometric and harmonic mean. The value can be assigned to different physical mechanisms of entropy production [14].
Like other previous works with Fluid$u$M [16], this thesis will use a value of $p = 0$ because it appears to provide the best description of Pb-Pb collisions. Moreover, $k = 1.4$ is used for the so-called fluctuation parameter, $\sigma = 0.6\,\mathrm{fm}$ for the nucleon width and $\sigma_\mathrm{inel}^\mathrm{NN} = 6.4\,\mathrm{fm}^2$ for the inelastic nucleon-nucleon cross section [14].

For the initial conditions used in this work, 5000000 minimum-bias events for the reduced thickness T_R were generated with random orientation in azimuthal direction and impact parameters $b \in \{0, 20\,\mathrm{fm}\}$. As the integral $\int T_\mathrm{R}(\vec{x})\,\mathrm{d}^2x$ is expected to be monotonically connected with the produced multiplicity of particles, this value can be used to group the generated events into centrality classes [16]. For the determination of the particle spectra and harmonic flow coefficients of the J/ψ this was implemented in 10% bins. It allows the important centrality dependence be taken into account while still having enough events of similar initial size in the transverse plane to describe them as an ensemble with random azimuthal orientation.
The initial entropy profile can be calculated for every centrality class individually by:

$$s(r) = \frac{\mathrm{Norm}}{\tau_0}\langle T_\mathrm{R}(r,\phi)\rangle \tag{2.2}$$

with an overall normalization norm where the initial proper time τ_0 was already excluded. This is because one expects an approximately linear decrease of the entropy density with the thermalization proper time due to the longitudinal expansion (Bjorken flow). In contrast to reference [16], it was decided to use one normalization for all centrality classes in this thesis. This choice comes closer to the idea of the T$_\mathrm{R}$ENTo model and avoids the risk of overfitting because of too many free parameters. A detailed justification is given in the analysis part.

The centrality bins implemented in the code often have a smaller binning than those

used for the experimental data. In order to produce results in the Fluid$u$M framework that can be compared to the data, the straightforward way would be to calculate e.g. the transverse momentum spectra first with the smaller binning, before they are combined to the larger bins. As this can be computationally rather expensive. the Fluid$u$M code does this in reversed order: It averages the corresponding entropy profiles to the desired broader centrality classes and uses those for the subsequent computations. Previous studies have shown that this simplification leads to only minor deviations of the order of 1% for the particle transverse momentum spectra [16]. This deviation is negligible with respect to the expected precision of our hydrodynamic modeling.

2.2. Hydrodynamic Evolution with Fluid$u$M

The system is locally described by a number of fluid dynamic fields, in this case the temperature T, the fluid velocity v, the shear stress π_η^η and π_ϕ^ϕ and the bulk viscous pressure π_{bulk}. These can be expressed as components of a „Nambu vector“ or „Nambu spinor“ $\mathbf{\Phi}$ [13].

This Nambu spinor depends generally on the Bjorken time τ, the radius r, the azimuthal angle ϕ and the rapidity y. Based on this general description, two statistical symmetries are applied: the Bjorken boost and the azimuthal symmetry. Both are not exact for a single event, but turn out to be very favorable with respect to the numerical effort. A sufficiently accurate description can now be achieved by a background-fluctuation splitting

$$\mathbf{\Phi}(\tau, r, \phi, y) = \mathbf{\Phi}_0(\tau, r) + \epsilon \mathbf{\Phi}_1(\tau, r, \phi, y) \tag{2.3}$$

with azimuthally symmetric background fields $\mathbf{\Phi}_0$ and perturbation fields $\mathbf{\Phi}_1$, which describe deviations from this symmetric situation [13]. The formal expansion parameter ϵ will be set $\epsilon \to 1$ in the end. In the current implementation of Fluid$u$M, only the terms in zeroth (corresponding to the symmetric background) and first order are considered in the end. Terms in quadratic or higher order are by construction much smaller and currently not included, their contribution might be implemented in a future version of Fluid$u$M .

This background-fluctuation mode is in fact very meaningful. The background parts of the fluid dynamic fields can be visualized as a characterization of the event average over many collisions with random azimuthal orientation. In contrast, the fluctuation

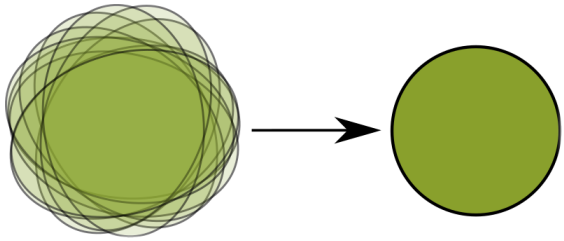

Figure 2.1.: Sketch of the background as an average of collisions with random azimuthal orientation. Figure taken from [18].

parts characterize event specific fluctuations [17]. Although the azimuthal symmetry is given for the event average regardless of the centrality, for the single event it is increasingly broken for more peripheral collisions. This corresponds to a larger perturbation contribution and a higher order perturbation terms could play an increasing role.

The second main technique of the framework to reach a higher numerical efficiency is a mode expansion of the perturbation fields. One uses two symmetry transformations. For azimuthal rotations $\phi \to \phi + \Delta\phi$, due to U(1) symmetry, the field configurations at fixed proper time τ can be described by a superposition of plane waves $e^{im\phi}$. From the underlying symmetry, it can be easily seen that the wave quantum number m is discrete with $m \in \mathbb{Z}$. Using the analogue for longitudinal boosts $y \to y + \Delta y$, the corresponding irreducible representations of translational symmetry are given by plane waves e^{iky} with the longitudinal wave number $k \in \mathbb{R}$.

The perturbation fields can now be expanded into Fourier modes [13]:

$$\mathbf{\Phi}_1(\tau, r, \phi, y) = \sum_{m=-\infty}^{\infty} \int \frac{\mathrm{d}k}{2\pi} e^{i(m\phi+ky)} \tilde{\mathbf{\Phi}}_1(\tau, r, \phi, y) \tag{2.4}$$

The fields are then given in Fourier space by $\tilde{\mathbf{\Phi}}_1(\tau, r, \phi, y)$ which is at fixed τ not only a function of the wave number k and m but also of the radius. For the characterization of initial conditions this radial dependence is also expressed in an expansion in terms of basis functions $q_{m,l}(r)$ with radial wave numbers l and fluctuating field amplitudes $\mathbf{h}_{m,l}$:

$$\tilde{\mathbf{\Phi}}_1(\tau_0, r, \phi, y) = \sum_l q_{m,l}(r) \mathbf{h}_{m,l}(k) \tag{2.5}$$

$$\overset{2.4}{\Rightarrow} \mathbf{\Phi}_1(\tau_0, r, \phi, y) = \sum_{m=-\infty}^{\infty} \sum_l \int \frac{\mathrm{d}k}{2\pi} e^{i(m\phi+ky)} q_{m,l}(r) \mathbf{h}_{m,l}(k) \tag{2.6}$$

In the current implementation polynomials are used as basis functions.

For the relativistic fluid dynamics, an equation of motion is directly inferred from energy and momentum conservation for the case of negligible net baryon number [13]. A relativistic viscous hydrodynamic approach based on the ideas of Müller as well as Israel and Stewart is applied [19, 20]. The applied numerical methods have been validated against the semi-analytic Gubser solution for Israel-Stewart type hydrodynamics as described in [13].

The thermodynamic equation of state (e.o.s.) is a function $p(T)$ from which all thermodynamic properties can be derived. This equation of state in the high temperature regime is known from lattice QCD results. For temperatures below the crossover to a gas dominated by hadronic degrees of freedom, results from a hadron resonance gas approach (HRG) are applied. Fluid$u$M uses a combination of exponential and rational functions, which allows a continuous crossover between both cases and provides sufficiently high regularity. The detailed function can be found in [13].

A central ingredient of the fluid dynamics is given by the implementation of the transport properties. In this thesis, a temperature independent value for the shear viscosity over entropy density η/s is assumed. This assumption is not self-evident and is an interesting subject for investigation. Nevertheless, a previous study on a temperature dependent η/s could not reach an improvement of the description of the ALICE experimental data compared to the temperature independent model [21]. Until now, no decisive conclusion about this question is known to the author, but the mentioned results can be seen as an indication that the temperature independent implementation used in this thesis is sufficient.

The bulk viscosity over entropy ratio ζ/s is parametrized as a Lorentz curve:

$$\frac{\zeta}{s} = \frac{(\zeta/s)_{\max}}{1 + \left(\frac{T - 0.175\,\mathrm{GeV}}{0.024\,\mathrm{GeV}}\right)^2} \tag{2.7}$$

with the bulk viscosity over entropy amplitude $(\zeta/s)_{\max}$. The parametrization as well as the width $(\zeta/s)_{\mathrm{width}} = 0.024\,\mathrm{GeV}$ and location $(\zeta/s)_{T_0} = 0.175\,\mathrm{GeV}$ of the Lorentz curve are taken from [22]. The bulk viscosity over entropy amplitude $(\zeta/s)_{\max}$ is not restricted to the value proposed in the cited reference, but can be used together with η/s, the freeze-out temperature T_{fo}, the initial proper time τ_0 and the normalization Norm as a fit parameter for the transverse momentum spectra modeling.

2.3. Freeze-Out

In the corresponding Fluid$u$M functions, the hadronization is implemented in as a sudden freeze-out at an adjustable temperature. The transition from the fluid dynamic fields to the final particle distribution is described by the Cooper-Frye formula [23]. According to it, the number of hadrons formed on the freeze-out hypersurface Σ given by

$$N = \int \frac{\mathrm{d}^3 p}{E_p} \int \mathrm{d}\Sigma_\mu(x) p^\mu f(x,p) \tag{2.8}$$

with the three-dimensional element of the freeze-out hypersurface $\mathrm{d}\Sigma_\mu(x)$ and the particle distribution function f. The latter is implemented in Fluid$u$M by the Fermi-Dirac or Bose-Einstein equilibrium distribution f_{eq} with shear corrections $\delta f_{\mathrm{shear}}$ and bulk corrections δf_{bulk} are applied:

$$f = f_{\mathrm{eq}} + \delta f_{\mathrm{shear}} + \delta f_{\mathrm{bulk}} \tag{2.9}$$

The detailed functional form of these correction is stated in [16] and is based on [24, 25].

In order to evaluate the Cooper-Frye formula 2.8, the Fluid$u$M code first calculates the one-dimensional shape freeze-out surface for given initial conditions, freeze-out temperature and fluid properties. The Fluid$u$M code uses the underlying symmetries in the model and the background-fluctuation splitting to make the calculations easier and faster than other hydrodynamic codes. The following tries to give an idea about the differences between Fluid$u$M and other hydrodynamic models. In figure 2.2, a plot of the freeze-out surface for $0-5\%$ centrality with a manually added equidistant azimuthal angle ϕ and the hypersurface elements (lightblue arrows) are shown. This plot only takes into account the background and is therefore (apart from the grid) totally symmetric in ϕ. The computation of the freeze-out surface takes only few minutes in Fluid$u$M which is by far faster than the corresponding time for other hydrodynamic models like MUSIC.

The shape in figure 2.2 is not only meant as a demonstration of hypersurface elements but rather as an attempt to bring the predictions from Fluid$u$M for the freeze-out surface in the same form as the MUSIC output in order to use existing codes to compare some results.

Interestingly, the output from this freeze-out surface leads to a quite different $\frac{\mathrm{d}N}{\mathrm{d}\beta}$ distribution as that from MUSIC calculations. This is shown in figure 2.3.

This has an interesting behavior of a nearly sharp cut-off for Fluid$u$M (left) in contrast

to a rather smooth distribution for MUSIC (right). The reason for this is not really much clear. Ideally, one would expect that both approaches lead to similar results. This has to be studied in more detail to draw conclusions about it. It should serve as a reminder in this section that differences between the approaches may exist and need to be investigated.

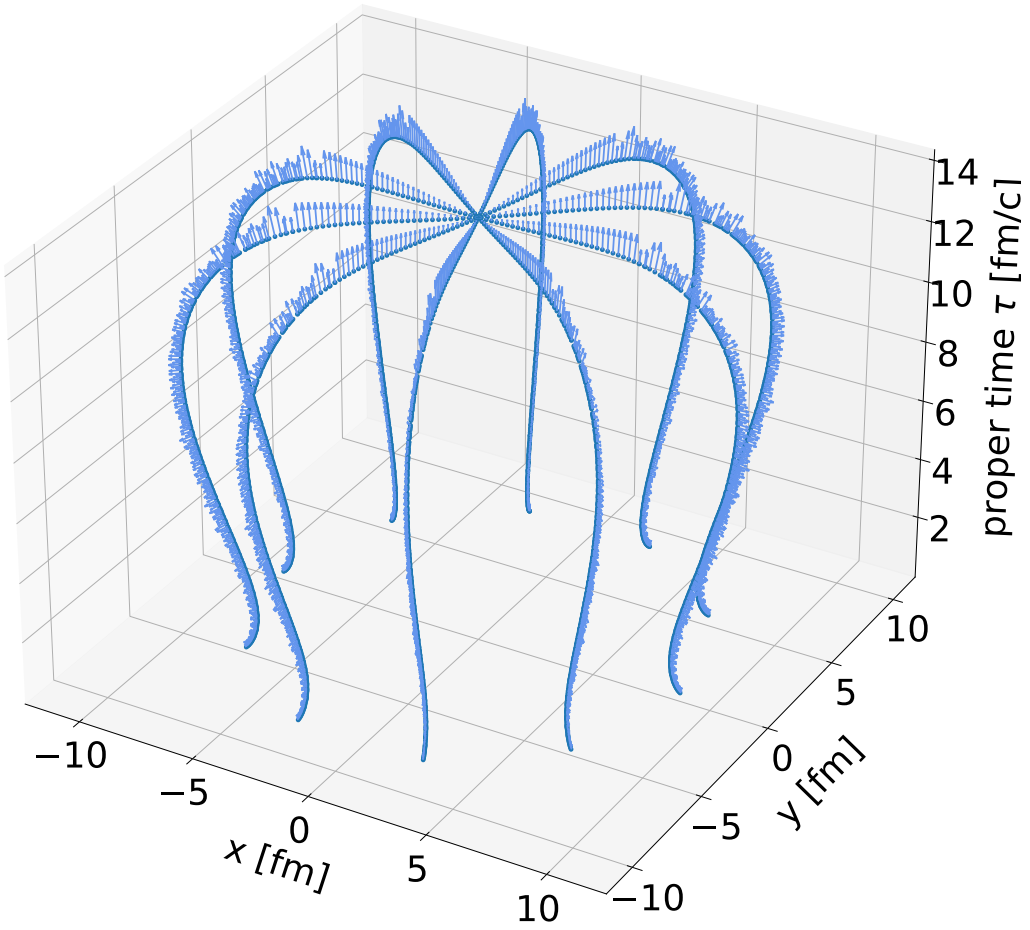

Figure 2.2.: 2+1 dimensional freeze-out hypersurface with arbitrary equidistant azimuthal angle grid based on the 1+1 dimensional freeze-out hypersurface from Fluid$u$M. The arrows correspond to the local hypersurface elements.

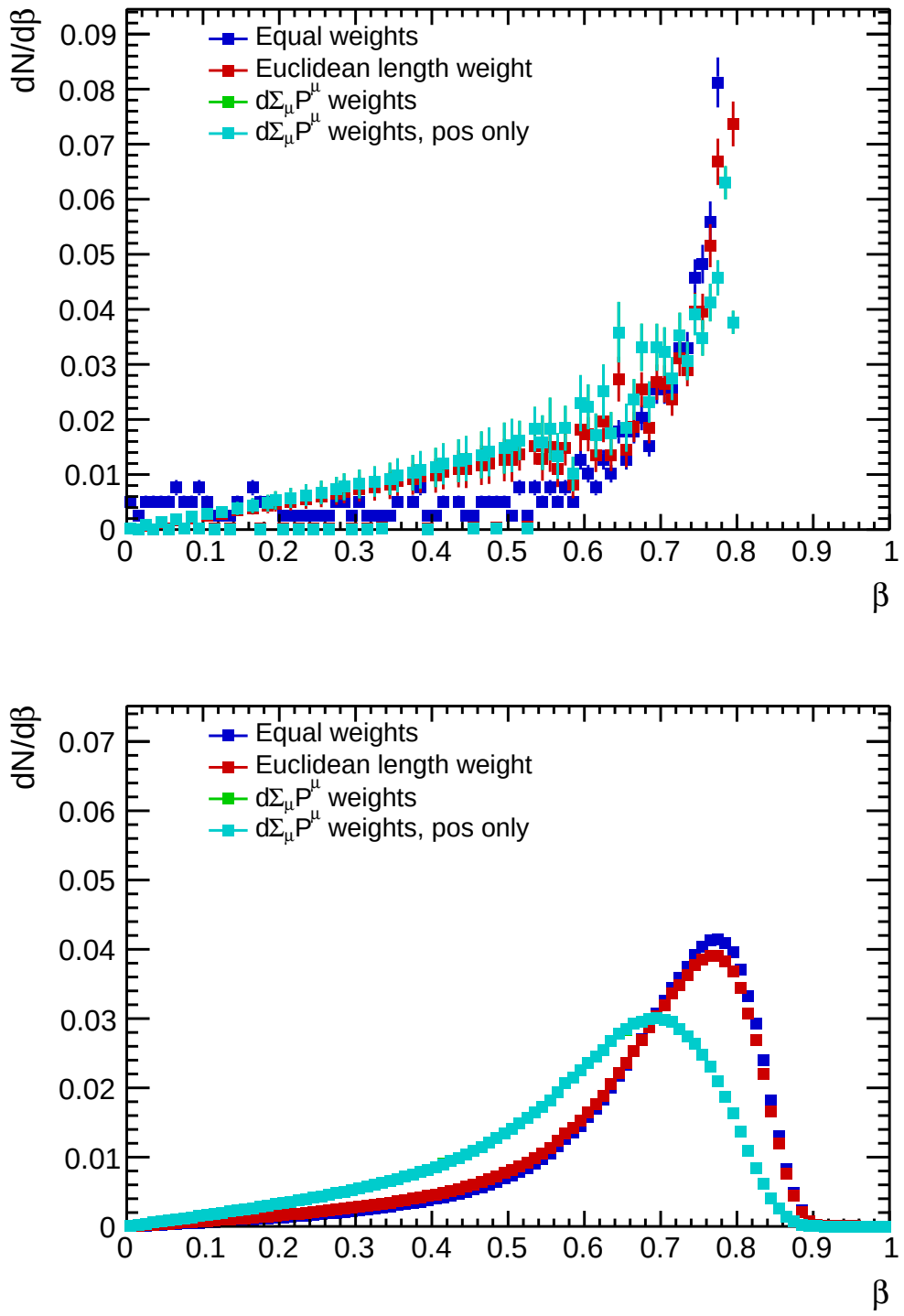

Figure 2.3.: $\frac{\mathrm{d}N}{\mathrm{d}\beta}$ as a function of β for Fluid$u$M (top) and MUSIC (bottom). The plots were produced by Martin Völkl based on the hypersurface elements shown in 2.2.

2.4. Resonance Decays with FastReso

The particles produced at the freeze-out need to be sufficiently long-lived to reach the detector instead of decaying on their way to it. These resonance decays from short-lived particles cause the feeddown: Short-lived particles decrease in abundance and populate through their decay products the states of certain long-lived particles.

This can obviously have enormous influence on the particle yields and consequently also on the transverse momentum spectra. The calculations to account for this, can be very lengthy. In the Fluid$u$M framework, the resonance decays are implemented by FastReso [15] which allows very efficient computations. The basic idea is that the decay maps are applied to the primary particle distribution before the the surface integral in 2.8 is computed. This way, the distribution functions can be pre-computed and saved as decay kernels so that the remaining equations can be calculated in a very short time [16]. The decay maps are based on the PDG Review of Particle Physics from 2016 [26], which provides a large set of resonance decays.

2.5. Statistical Hadronization Model

The basic idea of the statistical hadronization model is the description of the hadrons produced at the chemical freeze-out in a grand-canonical ensemble. In this framework, the system can be described by the corresponding partition function Z, from which all thermodynamic variables can be derived [27]. For temperatures lower than or equal to the temperature of the chiral phase transition T_c, the partition function can be approximated in the hadron resonance gas model. It can be decomposed into a mesonic and a baryonic part via

$$\ln\left[Z(T,V\mu)\right] \approx \sum_{i\in\text{mesons}} \ln\left[Z_{m_i}(T,V,\mu_Q,\mu_\text{s})\right] + \sum_{i\in\text{baryons}} \ln\left[Z_{m_i}(T,V,\mu_\text{b},\mu_Q,\mu_\text{s})\right] \quad (2.10)$$

with the masses m_i of the respective particles, the temperature T, the volume V of the central rapidity unit and the chemical potential $\mu = (\mu_\text{b}, \mu_Q, \mu_\text{s})$, which consists of a baryonic component, one from the electric charge and a strangeness component. The

partition function and the single particle density are given by the relations [12, 28]

$$\ln Z_i = \frac{V g_i}{2\pi^2} \int_0^\infty \pm p^2 \, \mathrm{d}p \ln[1 \pm \exp(-(E_i - \mu_i)/T)] \tag{2.11}$$

$$n_i = N_i/V = -\frac{T}{V} \frac{\mathrm{d} \ln Z_i}{\mathrm{d}\mu} = \frac{g_i}{2\pi^2} \int_0^\infty \frac{p^2 \, \mathrm{d}p}{\exp[(E_i - \mu_i)/T] \pm 1} \tag{2.12}$$

with $\mu_i = \mu_\mathrm{b} B_i + \mu_\mathrm{s} S_i + \mu_{I_3} I_i^3$ and (+) and (-) corresponding to fermions and bosons, respectively. With this description, values of $T_\mathrm{cf} = (156.5 \pm 1.5)\,\mathrm{MeV}$, $\mu_\mathrm{b} = (0.7 \pm 3.8)\,\mathrm{MeV}$ and $V = (5280 \pm 410)\,\mathrm{fm}^3$ were found [27] to give the best description of the particle yields measured by ALICE. The obtained value for the chemical freeze-out temperature T_fo is consistent within errors with the pseudo-critical temperature T_pc obtained from lattice QCD [29]. The baryon chemical potential reflects the expected equal production of matter and antimatter at the LHC [27].

For light flavor hadrons consisting of up (u), down (d) and strange (s) quarks, the calculated particle yields based on this statistical hadronization model could be described with an outstanding accuracy [27, 30, 31]. For heavy particles with $m \gg T_\mathrm{cf}$ and without considering resonance decays, the yield scales with the mass according to $m^{3/2} \exp(-m/T_\mathrm{cf})$.

2.5.1. Statistical Hadronization Model for Charmed Hadrons (SHMc)

For hadrons containing heavy-flavor quarks, a similar model can be applied. In contrast to the u, d and s quarks, the charm (c) and bottom (b) quarks have much higher masses $m > 1\,\mathrm{GeV}$, which are far above the pseudo-critical temperature T_c and are therefore strongly Boltzmann-suppressed [27]. Further, the masses are also higher than the QCD scale $\Lambda_\mathrm{QCD} = (332 \pm 17)\,\mathrm{MeV}$, which allows the application of perturbative QCD. Although thermalized production at the freeze-out is very small, hard scattering processes occur during the initial collision of the relativistic heavy-ions [27]. Between these scattering processes and the freeze-out, the heavy quarks strongly couple to the medium and reach, through these interactions, a sufficient degree of thermal equilibrium for the description with a thermal model. The central ideas and differences to the case of light flavor hadrons will be discussed here for hadrons containing charm quarks. For the bottom quark and the Υ meson as bottomonium, the concept can be extended in the same way.

In order to account for the absence of chemical equilibrium, a fugacity factor g_c is introduced. This factor accounts for charm conservation, which leads to the balance

equation [32], which describes the number of hadrons containing at least one charm or anti-charm quark:

$$N_{\mathrm{c\bar{c}}}^{\mathrm{dir}} = \frac{1}{2} g_{\mathrm{c}} V \left(\sum_i n_{D_i}^{\mathrm{term}} + n_{\Lambda_i}^{\mathrm{term}} + ... \right) + g_{\mathrm{c}}^2 V \left(\sum_i n_{\psi_i}^{\mathrm{term}} + ... \right) + ... \tag{2.13}$$

The first addend contains the thermal density n originating from open charm states (e.g. D mesons and Λ baryons), which contain one charm quark, while in the second addend the contributions from charmonium are contained. For the J/ψ , this implies a yield of

$$N_{\mathrm{J}/\psi}^{\mathrm{dir}} = g_{\mathrm{c}}^2 V n_{\mathrm{J}/\psi}^{\mathrm{term}} \tag{2.14}$$

and hence an enhancement of g_c^2 with respect to the expected thermalized yield (thermal density times volume). The fugacity factor can be determined using the charm balance equation 2.13. For central (0-10%) Pb-Pb collisions at $\sqrt{s_{\mathrm{NN}}}$ the fugacity has been determined as $g_{\mathrm{c}} = 29.5 \pm 5.2$, which implies a J/$\psi$ enhancement of about 900 [33]. This is shown on the left-hand side of figure 2.5.

This enhancement is in contrast to early predictions of a J/ψ suppression due to a color screening effect [34] similar to the Debye screening known from the electromagnetic interaction. For low beam energies, this screening effect leads to a suppressed production of J/ψ in heavy-ion collisions and the charm quarks will very likely form D mesons. However, for higher energies such as at the LHC, there are several charm anticharm quarks so that they may form charmonium at the freeze-out with charm quarks from different original pairs [33]. This mechanism is shown in figure 2.4 for low and high beam energies.

In order to describe the full p_{T} spectrum of charmed hadrons, a core-corona picture was developed [35]. The core part describes the central part of the collision where the density profile has sufficiently high values so that many collisions occur and a QGP is probably formed. For the outermost regions of the overlap this is not necessarily the case. The model assumes therefore no QGP to be formed when nucleons undergo one or less collisions. This condition corresponds to the nuclear density profile being below 10% of the central nuclear density. For the core part, a production according to the statistical hadronization considerations as discussed above. In contrast to that, the corona part behaves similar to a proton-proton collision where no QGP is assumed to be formed. A scaling by the number of binary nucleon-nucleon collisions is applied. [35]

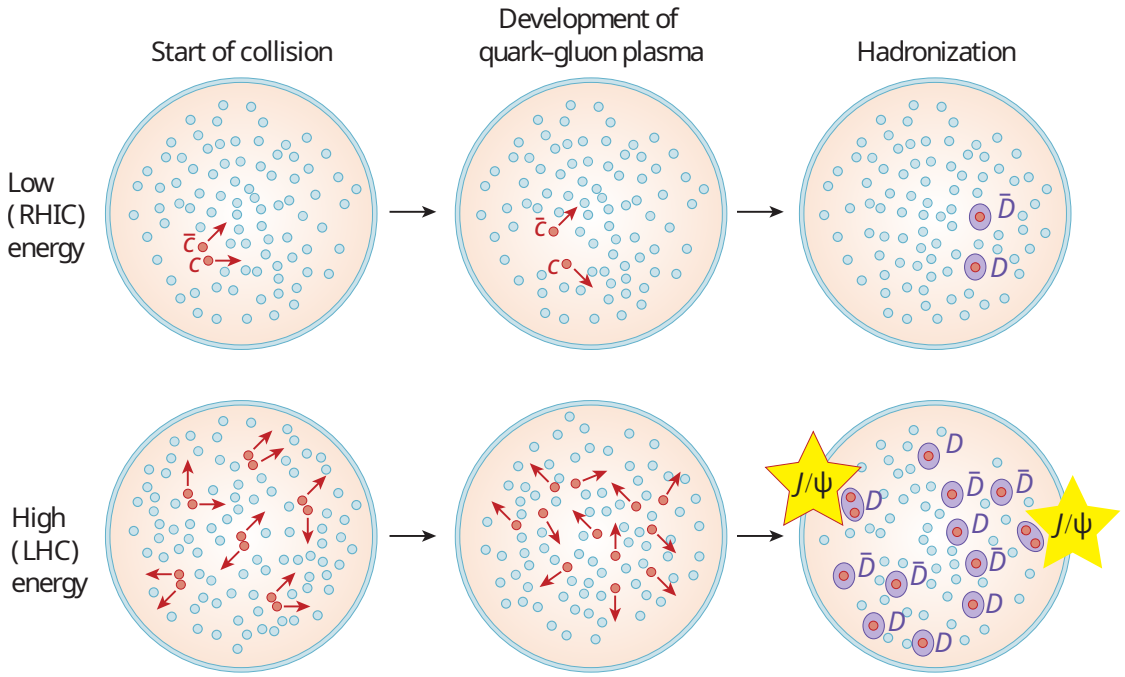

Figure 2.4.: The charm production and evolution until the hadronization is sketched. At the top, this is depicted for low collision energies, where only few charm-anticharm pairs are produced. The corresponding charm quarks are screened from each other and combine to D mesons at the freeze-out. In contrast at high energies, some charm quarks combine with anti-charm quarks from other pairs to J/ψ, which leads to an enhancement. Taken from [33].

In the case of the core part of the overlap region, the charm quarks thermalize with the medium and their total velocity is given by a superposition of the thermal motion and the velocity of the QGP medium, which can be obtained from hydrodynamic models [35]. The corona part of the p_{T} spectrum is obtained by a fit of

$$f(p_{\mathrm{T}}) = C \times \frac{p_{\mathrm{T}}}{(1 + (p_T/p_0)^2)^n} \tag{2.15}$$

to the transverse momentum spectra in pp collisions with p_0, n and C as fit parameters [35]. This description in a core-corona picture leads to transverse momentum spectra as shown on the right side of figure 2.5.

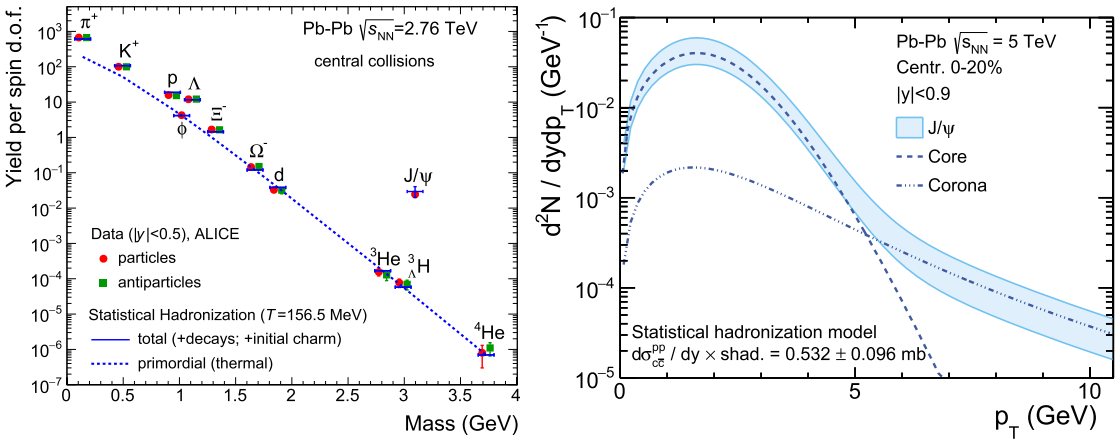

Figure 2.5.: Left: Description of the total particle yields in the central unit of rapidity with the statistical hadronization model. Right: Transverse momentum spectrum of J/ψ in the core-corona picture. Taken from [35]

.

3. Analysis and Results

Before a detailed study of the J/ψ is done in sections 3.4 and 3.5, the Fluid$u$M model will be tested for light flavor hadrons in sections 3.2 and 3.3. This is highly important for the assessment of its accuracy with respect to the experimentally rather well known transverse momentum spectra of pions, kaons and protons. In order to perform this analysis, the origin of the model parameters and the determination of the initial entropy normalization will be discussed in section 3.1.

3.1. Model Parameters and Determination of the Initial Entropy Normalization

A previous modeling analysis of ALICE data with Fluid$u$M applied a χ^2 minimization routine to determine best-fit parameters of T_{fo}, τ_0, η/s, $(\zeta/s)_{\mathrm{max}}$ and normalizations of the initial entropy profile Norm_i for the respective centrality classes [16].
The parameter fitting was done for experimental data from ALICE run 1 with a center-of-momentum energy per nucleon-nucleon pair of $\sqrt{s_{\mathrm{NN}}} = 2.76\,\mathrm{TeV}$, while this thesis will work with ALICE run 2 data at $\sqrt{s_{\mathrm{NN}}} = 5.02\,\mathrm{TeV}$. The increased beam energy has a relevant effect on the normalization Norm because the higher energy deposited in the collision region leads to an increase of the initial entropy.
Apart from this, the fundamental properties of the QGP itself are expected not to change substantially with the increase of beam energy. Therefore the obtained values for the four corresponding quantities, which are presented in table 3.1, will be used for the following analysis.

Based on unidentified charged hadron multiplicity, the analysis of global fluid fits [16] proposes also values for the normalization at $\sqrt{s_{\mathrm{NN}}} = 5.02\,\mathrm{TeV}$ of $\mathrm{Norm}_i = 75.6, 78.1, 77.8, 76.8, 76.4$ for the respective centrality classes.

Between the publication of the data cited above and this thesis, a bug was found in the Fluid$u$M code, which has been fixed now [36]. Therefore, the parameters should rather

be seen as a starting point for the analysis and the normalization of the entropy density profile needs to be determined separately.

The determination is done with a simple approach. The transverse momentum spectra are first calculated with Fluid$u$M for a certain normalization and can be compared to experimental data from [37]. Afterwards, the yield $\frac{\mathrm{d}N}{\mathrm{d}y}$ is determined for both experimental data and Fluid$u$M prediction. This is done by integration over the transverse momentum p_T using the trapezoidal rule. As the averaged charged-particle multiplicity is approximately proportional to the normalization of the initial entropy density [14], the same is also approximately fulfilled for the yield. This allows us to use a simple optimization approach for the normalization:

$$\mathrm{Norm}_\mathrm{new} = \mathrm{Norm}_\mathrm{old} \frac{(\mathrm{d}N \,/\, \mathrm{d}y)_\mathrm{data}}{(\mathrm{d}N \,/\, \mathrm{d}y)_\mathrm{model}} \tag{3.1}$$

Due to the monotonicity of the yield with respect to the normalization and the approximate linearity, the Norm converges after a few iterative executions.

In contrast to [16], only one parameter Norm for all centrality classes will be used in this thesis. This has two reasons: Firstly, the centrality dependence is already included in the initial state model T$_\mathrm{R}$ENTo. Therefore, the choice of different normalizations for all centrality classes would require indications that the description of centrality dependence in the initial state model is inadequate. Secondly, the usage of a centrality specific normalization does not lead to a significant improvement of the model prediction with respect to the experimental data. The influence is of the order of few percent for the particular centrality classes. This conclusion is drawn by executing the same procedure with a centrality-dependent normalization and can be found in appendix A. Furthermore, working with centrality-dependent normalizations would have increased the number of parameters from 5 to 9. This is not favorable because of both Occam's razor and the risk of overfitting.

3.2. Transverse Momentum Spectra of Light-Flavor Hadrons

Table 3.1.: Fluid$u$M Parameters used for the light hadrons

T_fo	τ_0	η/s	$(\zeta/s)_\mathrm{max}$	Norm
137.1 MeV	0.179 fm/c	0.164	0.059	69.55

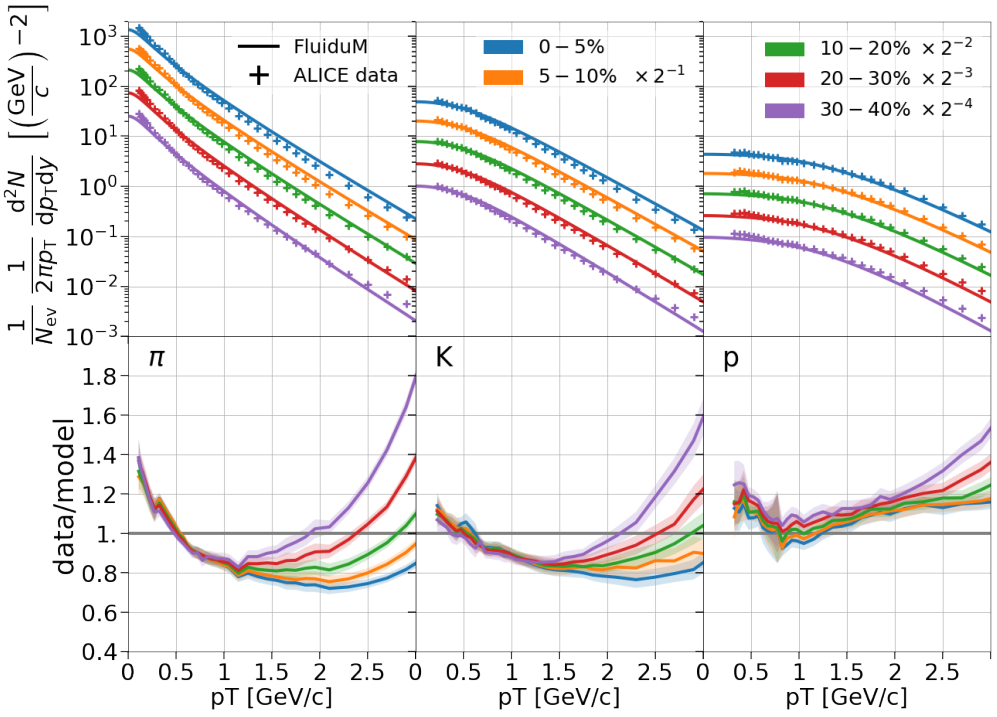

Figure 3.1.: Top: Predicted p_{T} spectra of pions, kaons and protons at $\sqrt{s_{\mathrm{NN}}} = 5.02\,\mathrm{TeV}$ together with the experimental data for $p_{\mathrm{T}} < 3\,\mathrm{GeV}/c$. Bottom: Illustration of the data to model ratio with uncertainties as shaded regions

For our analysis, the global initial entropy density normalization stated in table 3.1 was found. The experimental ALICE data are taken from [37], where the p_{T} spectra for both particles and antiparticles are represented simultaneously. As Fluid$u$M does not consider the antiparticles and due to the balance of particles and antiparticles at LHC energies [38, 39], the experimental data are divided by 2. The transverse momentum spectra of pion, kaon and proton are depicted in figure 3.1.

At the top, the corresponding values for experimental data and model prediction for the invariant yield are pictured as a function of the transverse momentum p_T. For a better distinctness, the curves were separated manually by a subsequent divisions by powers of 2. As the experimental uncertainties would not be clearly visible, they are only shown at the bottom of the figure. Resonance decays as well as corrections of the equilibrium (Bose-Einstein/Fermi-Dirac) distribution due to shear and bulk viscous dissipation are already taken into account in the model. The data over model ratio is pictured at the

bottom of the figure. The shaded regions around the lines represent the errors following from the data uncertainty. For the latter, the statistical and systematical uncertainties are added in quadrature: $\sigma = \sqrt{\sigma_{\mathrm{stat}}^2 + \sigma_{\mathrm{sys}}^2}$. It should be noted that Fluid$u$M does not provide an uncertainty of the model. Partly, this could be derived from the provided fit parameter errors. However, the model itself has also a systematic uncertainty especially in the p_{T} region where the hydrodynamic description reaches its limits of applicability. These will be covered in the following discussion.

The Fluid$u$M results show significant deviations from the experimental ALICE data, which cannot be explained with the data uncertainties. Moreover, the pions and kaons seem slightly underpredicted whereas the proton predictions are rather higher than the data. Nevertheless, the predictions are within 30% consistent with the data for all three considered particles over a wide range of transverse momentum.

Before going into more detail, one should note that the parameters are predicated on a χ^2 minimization for a Fluid$u$M version which still included a bug. Although these parameters technically cannot be expected to be best-fit parameters also for the Fluid$u$M version without bugs, the p_{T} spectra show a general accordance with the course of the data points despite its variation over more than 3 decades within the considered p_{T} interval. As the current values are not yet fully optimized, the deviations could be further reduced by repeating the χ^2 optimization routine for the current Fluid$u$M implementation. Work on optimizing the modeling of Fluid$u$M is already in progress [40] and future results will show if the slight one-sided deviations for the individual particles vanish for the resulting parameter set.

Apart from this, the model prediction and its corresponding deviation from the data is similar to other hydrodynamic models and shows some well-known features.
Firstly, the pion prediction exhibits a striking enhancement at low p_{T}. This property was found in various models and is still an unsolved puzzle since many years [41–45]. Some previous attempts to explain this feature relied on insufficient implementation of resonance decays. Although this work incorporates a large number of resonance decays due to FastReso, this enhancement at low p_{T} remains. Moreover, there could be found no substantial improvement of Fluid$u$M predictions when including a larger set of resonance decays [16]. The same reference mentions finite widths of resonance decays, pion condensation and higher-order viscous corrections as recent investigations on this behavior.
Secondly, the spectra of all three particle increase dramatically at high p_{T}. It can be

seen that the increase is very distinctive for pions and the least dominant for protons. This phenomenon can be related to the applicability of the hydrodynamic description and accordingly that of the thermal production. For a high transverse momentum, the contribution from hard partons from the initial hard scatterings which do not fully thermalize play a dominant role in the p_{T} spectrum. This effect appears for pions already at a lower p_{T} than in the case of kaons or protons which reflects the mass ordering of the three particles.

Furthermore, this effect is more dominant for more peripheral collisions. Within the statistical hadronization model, this can be related to the growing corona fraction with increasing value of centrality so that the proton-proton like spectrum gains a stronger influence. In contrast to that, the most central collisions are predominantly determined by the core part. One can also explain it with the typically lower distance between the vertex of initial scatterings and the edge of the QGP so that the produced particles may not have enough time to thermalize with the medium and remain with a high momentum.

Interestingly, some previous analyses of transverse momentum spectra proposed a phase of hadronic re-scatterings („hadronic afterburner“) as part of a gradual freeze-out after the hydrodynamic evolution to gain a better description of the proton p_{T} spectra at $p_{\mathrm{T}} < 1\,\mathrm{GeV}/c$ [46–48]. However, in the results presented above, the proton p_{T} spectra are fairly well described within about 20%, have a very flat distribution over the p_{T} range and therefore show no clear indications that the Fluid*u*M description with a sudden freeze-out is insufficient. The slight increase at lower transverse momentum around $0.5\,\mathrm{GeV}/c$ is an interesting feature, but not as remarkable as one might have expected from [47]. It is an interesting question how this behaves when a renewed parameter optimization has been applied in the current Fluid*u*M implementation.

In conclusion, the Fluid*u*M framework provides a very reasonable description of the data regarding that the model itself has a presently unconsidered uncertainty and that a parameter optimization may fix some of the slight deviations. The general shape of the spectra are for a wide p_{T} interval in accordance with the data and the most apparent features at high p_{T} or for pions at low p_{T} can be either explained or are well known from every other currently known hydrodynamic description, respectively. Taking this into account, the remaining inaccuracies of the model of the order of approximately 20% are still acceptable for the further analysis.

3.3. Elliptic Flow of Light-Flavor Hadrons

In order to assess the accuracy of the calculated elliptic flow v_2 in Fluid$u$M, the v_2 for $p_T < 3\,\mathrm{GeV}/c$ are compared to experimental data from the ALICE collaboration for $|y| < 0.5$ [11]. Both are depicted in figure 3.2 with errors calculated as the systematic and statistical errors added in quadrature; resonance decays are already considered in the model.

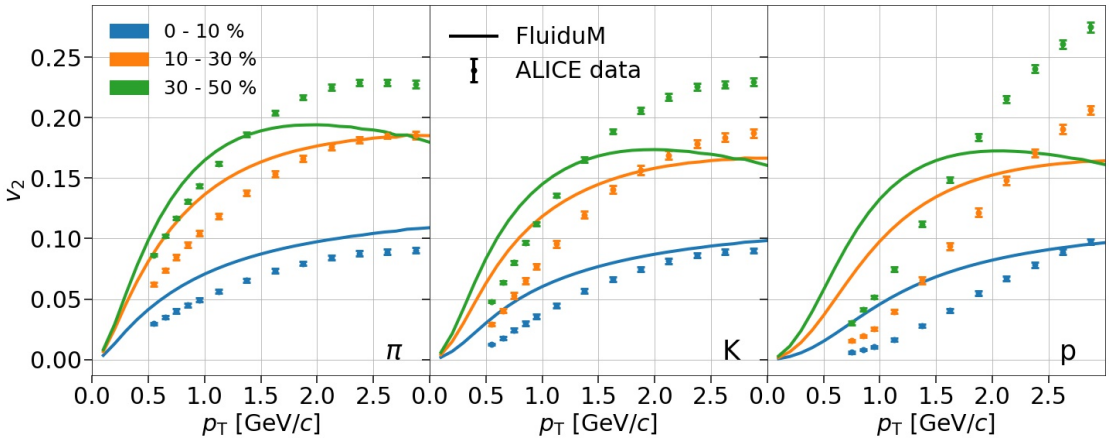

Figure 3.2.: Fluid$u$M prediction and experimental data of elliptic flow v_2 as a function of the transverse momentum for pions (left), kaons (middle) and protons (right)

For the pions and kaons, the model a qualitatively good agreement with the data points, although it can not provide sufficiently high accuracy to describe the data points within their uncertainties. For all particles, this description is much better in the $0-10\%$ and $10-30\%$ centrality class than in more peripheral collisions with $30-50\%$ centrality. Moreover, the data are overestimated at low p_T and rise to a similar level of the prediction or even exceed it at higher p_T. Whats is striking in this figure are the differences between data and model for the protons. The overestimation at low and underestimation at high p_T is the most evident here and while the Fluid$u$M predication seems to reach its peak at or close to the shown p_T range, the data is still increasing with p_T .

For the discussion of these results, it should be noted that for the moment, the anisotropic flow coefficients calculated by Fluid$u$M have to be regarded with a bit of caution. Due to a change in the used basis functions from Bessel functions to the current implementations with polynomials, there is still a minor bug remaining in the code for the v_n calculation. This bug is probably manifested in an enhancement of a factor 5.068, which is the inverse

of $\hbar c \approx 0.197\,\mathrm{GeV\,fm}$ occurring due a unit conversion in the code [36]. This factor has already been divided in figure 3.2. Comparing the prediction to the data, this attempt to fix the bug leads to a reasonable magnitude of the elliptic flow and provides results that are mostly compatible with the data.

The large deviations for higher centrality classes could be an effect of considering perturbations only up to the first order. In the limit of the most central events, azimuthal symmetry is apart from fluctuations even for the single event approximately existent and the perturbation contribution can be expected to be small. In contrast to that, in more peripheral events, the fluctuation gains in importance and quadratic order perturbation terms may be necessary. Presently no evaluation of this effect are known to the author and it could be an interesting subject for future studies.

3.4. J/ψ Transverse Momentum Spectra

The same procedure can be repeated for the J/ψ with some adjustments. For the J/ψ, resonance decays do not need to be considered because of their negligible contribution to the spectra. As explained in the section 2.5, the production of charmonium is very much different to that of light flavor hadrons like pions, kaons and protons.

The charm quarks are produced in the initial hard collisions and thermalize with the medium during the evolution of the QGP. When chemical freeze-out is reached, these charm quarks form either D mesons or charmonium states. The chemical freeze-out temperature is known from analyses based on the statistical hadronization model to happen at $156.5 \pm 1.5\,\mathrm{MeV}$ [27]. Therefore, a compatible freeze-out temperature of $T_{\mathrm{fo}} = 156\,\mathrm{MeV}$ is used in Fluid$u$M.
For the production of J/ψ, conservation of the charm and anticharm quarks produced in the initial hard scattering must be considered. This makes it rather different to the thermal production of light flavor hadrons and leads to the observed charm enhancement, which was predicted by the SHM [49]. Hence, the p_{T} spectra need to be scaled to fit the J/ψ enhancement.

The yield of the core part of the p_{T} spectrum has been quantified based on the SHM model to $\mathrm{d}N\,/\,\mathrm{d}y = 0.122$ ([50], updated values from [51]). The obtained thermal p_{T} spectrum was scaled to this yield, which leads to the curve shown in figure 3.3. The corona contribution, obtained as described in [35] and scaled to a yield of $\mathrm{d}N\,/\,\mathrm{d}y = 0.00525$ [50, 51], is plotted and added to the predicted core p_{T} spectrum in order to get

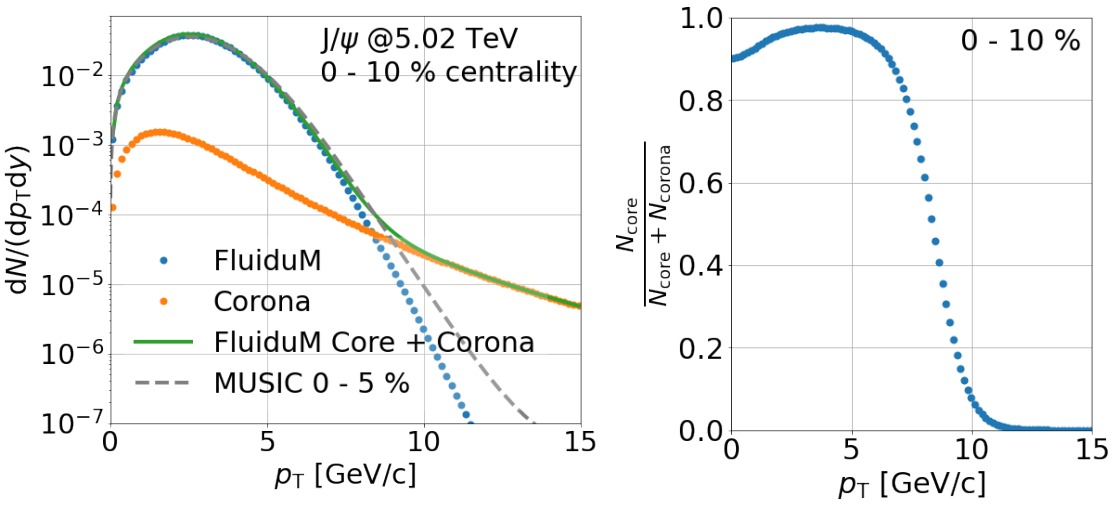

Figure 3.3.: Left: J/ψ p_{T} spectrum of the core part based on Fluid$u$M results (blue dots) plotted together the corona contribution (orange dots), which leads to the resulting J/ψ p_{T} spectra (green solid line) for $0-10\%$ centrality. As a reference, the result for the core contribution for $0-5\%$ centrality based on a hydrodynamic evolution with MUSIC (dashed gray line) is presented. Right: Fraction of the core part to the total spectrum as a function of p_{T}.

the total p_{T} spectrum. A result based on a similar calculation with MUSIC [9] for the hydrodynamic modeling is presented in gray [52]. The portion of the core contribution is depicted on the right-hand side as a function of the transverse momentum. It should be noted that the MUSIC core part is for $0-5\%$ centrality in contrast to the other curves, which might also lead to small deviations.

This leads to a reasonable curve that has a peak close to 3 GeV and is dominated by the core contribution until approximately 8 GeV. The description is very similar to that obtained with MUSIC although the tail of the core contribution is shifted towards a slightly higher p_{T}.

The same procedure is repeated for the $30-50\%$ centrality class with a core yield of $\mathrm{d}N\,/\,\mathrm{d}y = 0.0117$ and a corona yield of $\mathrm{d}N\,/\,\mathrm{d}y = 0.00259$. The result is shown in figure 3.4.

The first thing that can be noticed is that the used core yield is much smaller than for the more central collisions. Especially, the core fraction is also generally lower throughout the p_{T} range and falls off earlier. This is clearly evident from the collisiongeometry, as

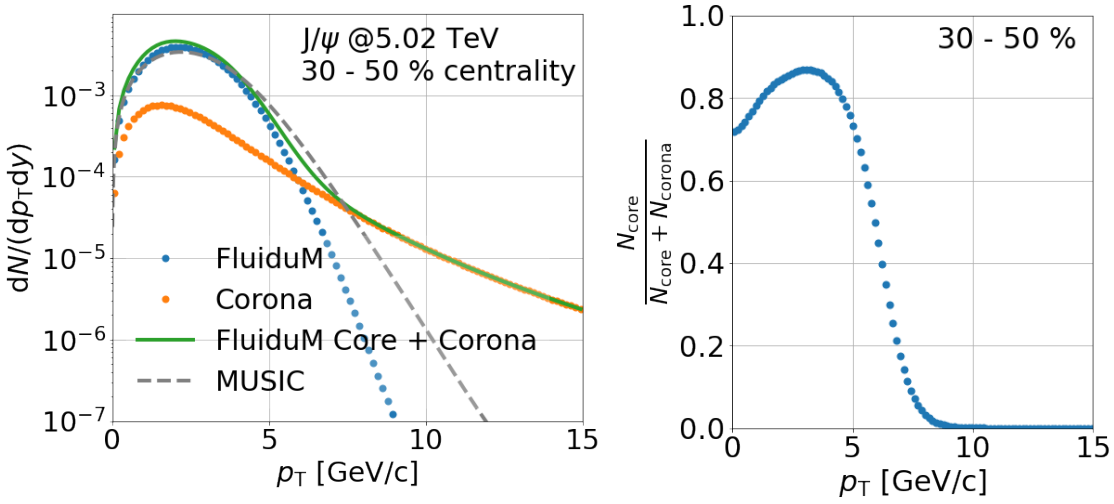

Figure 3.4.: Left: J/ψ p_{T} spectrum of the core part based on Fluid$u$M results (blue), the corona contribution (orange) and the resulting J/ψ p_{T} spectra (green) for $30-50\%$ centrality with MUSIC results (grey) as comparison. Right: Fraction of the core part to the total spectrum as a function of p_{T}.

there are relatively more pp-like events corresponding to particles undergoing at most one collision for a very peripheral overlap. Additionally, the difference between Fluid$u$M and MUSIC results is much larger than in the $0-10\%$ centrality class and has a very relevant effect on the overall spectrum. It is again an interesting question what effects may originate from higher order perturbation terms.

3.5. J/ψ Anisotropic Flow Coefficients

Analogously to the discussed results for anisotropic flow of light flavor hadrons, these coefficients can be calculated also for the J/ψ neglecting resonance decays.
In order to account for the corona and core parts of the spectra, the v_2 of the core is multiplied with the fraction of the core contribution at the respective transverse momentum (shown on the right-hand side of 3.3 and 3.4). This causes a drop-off of the resulting v_2 distribution for high transverse momenta where the corona dominates. In figure 3.5, these results are compared to data from forward rapidity, which can still serve as a reference due to a sufficiently fulfilled Bjorken boost symmetry. For both $0-10\%$ and $30-50\%$ centrality, significant deviations from the data can be observed. Currently, the results from MUSIC provide a better description of the data and the Fluid$u$M re-

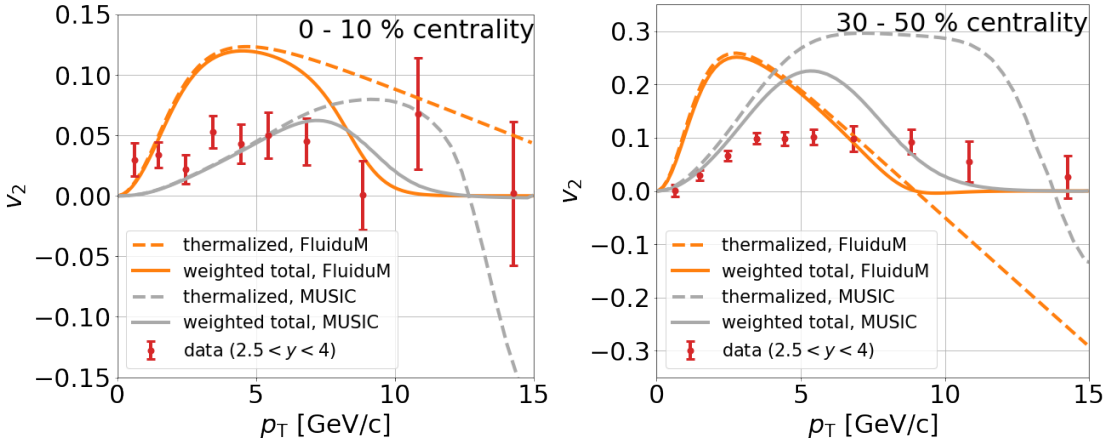

Figure 3.5.: The elliptic flow as a function of the transverse momentum for very central (left) and more peripheral (right) collisions. The Fluid$u$M (orange dots) and MUSIC (gray dashed line) results with and without the weights from the core fraction as well as the experimental data (red errorbars) are depicted.

sults have a peak at much lower p_T. Interestingly, for $30-50\%$ centrality both models predict a negative v_2 for high transverse momenta (which is suppressed by the small core fraction).
The difference between the Fluid$u$M and MUSIC description may seem quite surprising and at the moment, no obvious explanation for this has been found. The rather sharp drop-off in the $\mathrm{d}N\,/\,\mathrm{d}\beta$ distribution presented in chapter 2.3 have already shown that there are some differences between the results of both models. The small differences in the predictions for the J/ψ spectra in the central events are therefore not very much surprising, but for the moment the tremendously different v_2 distributions cannot be fully explained.

The results of the same routine for the triangular flow are depicted in figure 3.6. Also v_3 seems to be overestimated by the model, especially for peripheral events where the triangular flow data are very close to or even compatible with zero.

The general expectation that the anisotropic flow coefficients decrease with the order is fulfilled for both centrality classes, although it is only a slight decrease in the case of the central $0-10\%$ events.

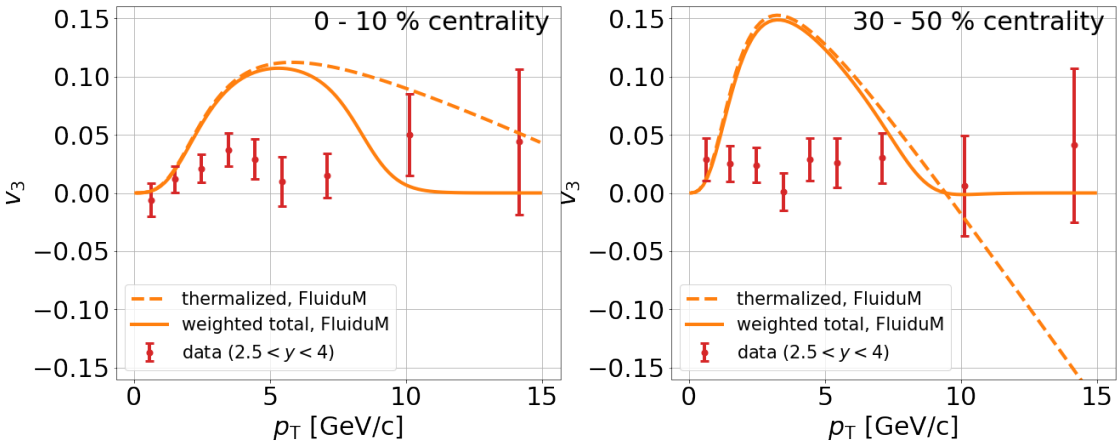

Figure 3.6.: The triangular flow as a function of p_T for very central (left) and more peripheral (right) collisions. The Fluid$u$M (orange) are shown with (solid line) and without (dashed line) the corresponding core weights and are compared to experimental data.

4. Summary and Conclusion

In this thesis, the hydrodynamic modeling with Fluid$u$M of the quark gluon plasma produced in the relativistic heavy-ion collisions at the LHC was examined. Fluid$u$M is a fluid dynamic approach that uses of a background-fluctuation splitting and a mode expansion of the perturbation. This technique has the main advantage that it allows a high numerical efficiency so that each single evaluation can be done much more than one order of magnitude faster than with other hydrodynamic programs and without needing much computing power. This is in fact more than just a convenient feature, it is a very valuable property as time is a human resource that can be very scarce in scientific researches.

In order to assess also the accuracy of the model in predicting the central observables of heavy-ion collisions, the p_{T} spectra and the elliptic and triangular flow were calculated for light flavor hadrons, namely pions, kaons and protons. These values were compared to the rather well-known experimental data from the ALICE experiment.

For this analysis, parameter values from a previous χ^2 minimization routine [16] were used and the corresponding normalization of the initial entropy density profile was adapted to the total yield. For this, it emerged that the use of one normalization for the entropy profiles of all centrality classes seemed more reasonable.

The results provided a quite good description of the p_{T} spectra for all centrality classes and all three particle within mostly $20-30\%$. Nevertheless, for the sake of completeness, it should be noted that the necessary accuracy for describing the experimental data within their uncertainties cannot be achieved. Although these spectra have been known for many years to a sufficiently high accuracy, they are still not fully understood and contain puzzling and interesting behaviors such as the pion spectra at low transverse momentum. This striking behavior, also known as the pion enhancement at low p_{T}, which could not been explained yet, is also very strong present in this analysis in spite of the larger number of resonance decays that have been taken into account.
Moreover, another apparent feature could be found at higher p_{T} where the data is

significantly underestimated. This can be related to the contribution of initial hard scatterings to the spectra that cannot be described by relativistic hydrodynamics. For the p_{T} spectra, improvements can be made when new parameters are known from an optimization of the particle spectra for the current Fluid$u$M version. Though the used parameter set lead (under these circumstances) to astonishingly reasonable results, this optimization is necessary to assess how much these p_{T} spectra can still improve.

The general shape of the v_2 spectra for light hadrons is also reasonably described by the model, but tends to show a peak at a lower transverse momentum, which leads to an overestimation in the low p_{T} region and an underestimation at higher p_{T}. This discrepancy is especially distinct for the protons. With regard to the anisotropic flow, it should be noted that there is still a remaining bug in the code, that is assumed to be fixed by the multiplication with a factor of $\hbar c$ and could not be corrected in the code before the submission of this thesis. This bug is about to be fixed very soon, which will hopefully verify the validity of the results for the elliptic and triangular flow. However, this reflects also that the development of Fluid$u$M is still in progress.

An interesting question for the p_{T} spectra and the anisotropic flow coefficients concerns quadratic orders of perturbation. These have a contribution to the predicted observables that may be included in future versions of Fluid$u$M. It would be interesting information how substantially they contribute to the spectra.

For the J/ψ p_{T} spectra, the gained spectra at the chemical freeze-out temperature of $T_{\mathrm{fo}} = 156\,\mathrm{MeV}$ from Fluid$u$M have been scaled to the predicted J/ψ core yield. After this, they were added to the corona distribution which is similarly based on results for pp measurements. For the central $0 - 10\%$ centrality class, the presented model gives very similar results as the hydrodynamic simulation with MUSIC in 2+1D and only a slightly longer tail towards high transverse momentum is observable. For the more peripheral results, the difference was substantially higher, raising open questions about the origins of this behavior.

The v_2 distribution are also rather overestimated with respect to the data and have a peak at lower p_{T} than predicted by MUSIC. The interesting feature that the v_2 prediction becomes negative at high transverse momentum occurs for both models in the more peripheral collisions.
The triangular flow has similar properties. As expected, the v_3 is smaller than the v_2, but only slightly for the central and distinctly smaller for the peripheral collisions.

All in all, the p_{T} spectra for light flavor hadrons seem to be well described by the Fluid$u$M framework. Also the obtained J/ψ p_{T} spectrum for $0-10\%$ centrality is similar to that from MUSIC. For the peripheral collisions the differences between both models increase.

Appendices

A. Centrality-Dependent Initial Entropy Density Profile Normalizations

The transverse momentum spectra for pions, kaons and protons can also be calculated for centrality-dependent normalizations. Performing a yield optimization routine according to (3.1) for Norm_i leads to the following results; the centrality classes are denoted by $i \in \{1, 2, 3, 4, 5\}$ corresponding to 0-5%, 5-10%, 10-20%, 20-30% and 30-40% centrality. The obtained entropy density profile normalizations are presented in table A.1. One can

Table A.1.: Centrality-dependent entropy density profile normalizations Norm_i

Norm_1	Norm_2	Norm_3	Norm_4	Norm_5
69.18	69.20	69.53	70.46	70.67

see that the norm increases slightly with the centrality, which can be associated to the stronger influence of jet quenching. If the model has these additional free parameters, our routine scales the normalization in order to fit the enhancement at high p_T better. This can be seen as hint that the slight variation of the normalization with the centrality leads to no significant improvement of the description of the p_T spectra. Having a closer look at the resulting spectra (figure A.1) indeed, no substantial differences can be found compared to the spectra with a centrality independent entropy normalization. The comparison serves as a further justification of our model with fewer parameters.

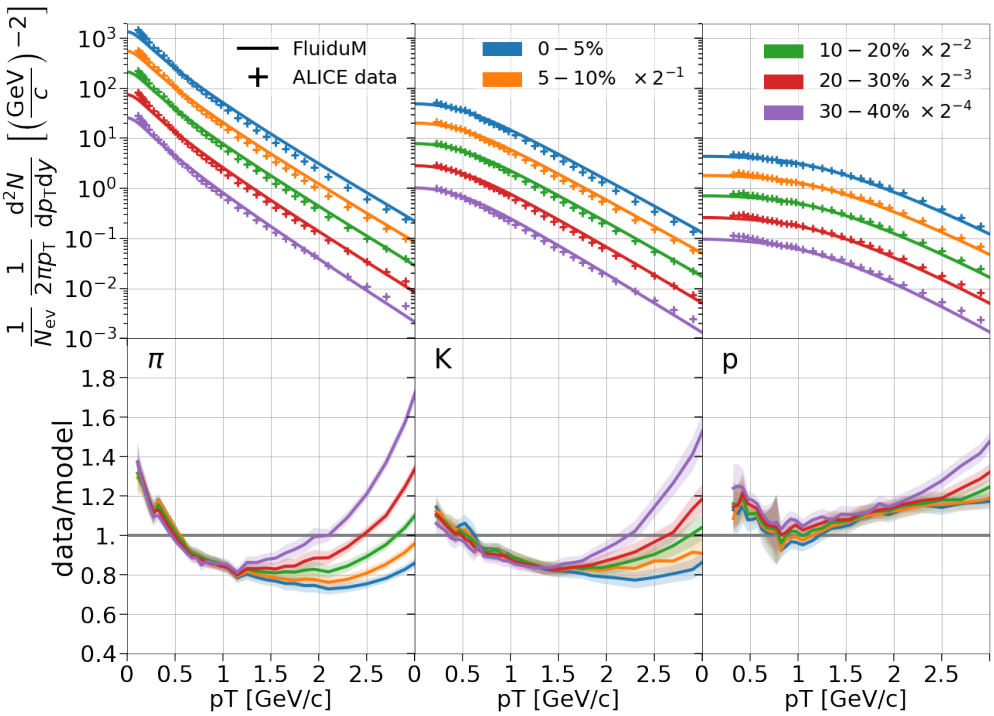

Figure A.1.: Top: p_{T} spectra of pions, kaons and protons at $\sqrt{s_{\mathrm{NN}}} = 5.02\,\mathrm{TeV}$ for a centrality-dependent entropy density normalization together with the experimental data for $p_{\mathrm{T}} < 3\,\mathrm{GeV}/c$. Bottom: Illustration of the data to model ratio with uncertainties as shaded regions

Bibliography

1. Heinz, U. W. *Concepts of Heavy-Ion Physics* 2004. https://arxiv.org/abs/hep-ph/0407360.
2. Boyanovsky, D., de Vega, H. & Schwarz, D. Phase Transitions in the Early and Present Universe. *Annual Review of Nuclear and Particle Science* **56,** 441–500. https://doi.org/10.1146/annurev.nucl.56.080805.140539 (Nov. 2006).
3. McInnes, B. A Rotation/Magnetism Analogy for the Quark Plasma. *Nuclear Physics B* **911,** 3 (Apr. 2016).
4. Florkowski, W. *Phenomenology of Ultra-Relativistic Heavy-Ion Collisions* ISBN: 978-981-4280-66-2 (Mar. 2010).
5. Chatrchyan, S. *et al.* Measurement of the elliptic anisotropy of charged particles produced in PbPb collisions at $\sqrt{s_{NN}} = 2.76$ TeV. *Phys. Rev. C* **87,** 014902. https://link.aps.org/doi/10.1103/PhysRevC.87.014902 (1 Jan. 2013).
6. Jacak, B. V. & Muller, B. The exploration of hot nuclear matter. *Science* **337,** 310–314. https://rhig.physics.yale.edu/Summer2014/Jacak_Mueller.pdf (2012).
7. Kovtun, P. K., Son, D. T. & Starinets, A. O. Viscosity in Strongly Interacting Quantum Field Theories from Black Hole Physics. *Phys. Rev. Lett.* **94,** 111601. https://link.aps.org/doi/10.1103/PhysRevLett.94.111601 (11 Mar. 2005).
8. Luzum, M. & Romatschke, P. Conformal relativistic viscous hydrodynamics: Applications to RHIC results at $\sqrt{s_{NN}} = 200$ GeV. *Phys. Rev. C* **78,** 034915. https://link.aps.org/doi/10.1103/PhysRevC.78.034915 (3 Sept. 2008).
9. Gale, C., Jeon, S., Schenke, B., Tribedy, P. & Venugopalan, R. Event-by-Event Anisotropic Flow in Heavy-ion Collisions from Combined Yang-Mills and Viscous Fluid Dynamics. *Physical Review Letters* **110.** https://doi.org/10.1103/physrevlett.110.012302 (Jan. 2013).

10. Castellanos, J. C., Grosa, F. & Völkl, M. A. Going with the flow. *Cern Courier.* https://cerncourier.com/a/going-with-the-flow/ (Apr. 2021).

11. Acharya, S. *et al.* Anisotropic flow of identified particles in Pb-Pb collisions at $\sqrt{s}_{\mathrm{NN}} = 5.02$ TeV. *JHEP* **09,** 006. arXiv: 1805.04390 [nucl-ex] (2018).

12. Reygers, K. & Stachel, J. *Lecture notes: Quark-Gluon Plasma Physics, 5. Statistical Hadronization and Strangeness* 2019. https://www.physi.uni-heidelberg.de/~reygers/lectures/2019/qgp/qgp2019_05_stat_stra.pdf.

13. Floerchinger, S., Grossi, E. & Lion, J. Fluid dynamics of heavy ion collisions with mode expansion. *Physical Review C* **100.** https://doi.org/10.1103/physrevc.100.014905 (July 2019).

14. Moreland, J. S., Bernhard, J. E. & Bass, S. A. Alternative ansatz to wounded nucleon and binary collision scaling in high-energy nuclear collisions. *Phys. Rev. C* **92,** 011901. https://link.aps.org/doi/10.1103/PhysRevC.92.011901 (1 July 2015).

15. Mazeliauskas, A., Floerchinger, S., Grossi, E. & Teaney, D. Fast resonance decays in nuclear collisions. *The European Physical Journal C* **79.** https://doi.org/10.1140/epjc/s10052-019-6791-7 (Mar. 2019).

16. Devetak, D. *et al.* Global fluid fits to identified particle transverse momentum spectra from heavy-ion collisions at the Large Hadron Collider. *JHEP* **06,** 044. arXiv: 1909.10485 [hep-ph] (2020).

17. Floerchinger, S. & Wiedemann, U. A. Kinetic freeze-out, particle spectra, and harmonic-flow coefficients from mode-by-mode hydrodynamics. *Phys. Rev. C* **89,** 034914. https://link.aps.org/doi/10.1103/PhysRevC.89.034914 (3 Mar. 2014).

18. Kirchner, A., Giacalone, G., Grossi, E., Floerchinger, S. & Capellino, F. *Precision hydrodynamic predictions for particle production in isobar collisions at RHIC* in (Apr. 6, 2022). https://indico.cern.ch/event/895086/contributions/4712145/.

19. Müller, I. Zum Paradoxon der Wärmeleitungstheorie. *Zeitschrift für Physik* **198,** 329–344. ISSN: 0044-3328. https://doi.org/10.1007/BF01326412 (Aug. 1967).

20. Israel, W. & Stewart, J. Transient relativistic thermodynamics and kinetic theory. *Annals of Physics* **118,** 341–372. ISSN: 0003-4916. https://www.sciencedirect.com/science/article/pii/0003491679901301 (1979).

21. Sonnabend, C. *On the influence of temperature-dependent η/s on transverse-momentum particle spectra in heavy-ion collisions* 2020. https://www.physi.uni-heidelberg.de/Publications/ChristianSonnabend_BachelorThesis.pdf.

22. Moreland, J. S., Bernhard, J. E. & Bass, S. A. Bayesian calibration of a hybrid nuclear collision model using p−Pb and Pb-Pb data at energies available at the CERN Large Hadron Collider. *Phys. Rev. C* **101,** 024911. https://link.aps.org/doi/10.1103/PhysRevC.101.024911 (2 Feb. 2020).

23. Cooper, F. & Frye, G. Single-particle distribution in the hydrodynamic and statistical thermodynamic models of multiparticle production. *Phys. Rev. D* **10,** 186–189. https://link.aps.org/doi/10.1103/PhysRevD.10.186 (1 July 1974).

24. Teaney, D. Effect of shear viscosity on spectra, elliptic flow, and Hanbury Brown–Twiss radii. *Phys. Rev. C* **68,** 034913. https://link.aps.org/doi/10.1103/PhysRevC.68.034913 (3 Sept. 2003).

25. Paquet, J.-F. *et al.* Production of photons in relativistic heavy-ion collisions. *Phys. Rev. C* **93,** 044906. arXiv: 1509.06738 [hep-ph] (2016).

26. Olive, K. Review of Particle Physics. *Chinese Physics C* **40,** 100001. https://doi.org/10.1088/1674-1137/40/10/100001 (Oct. 2016).

27. Andronic, A., Braun-Munzinger, P., Redlich, K. & Stachel, J. Decoding the phase structure of QCD via particle production at high energy. *Nature* **561,** 321–330. https://doi.org/10.1038/s41586-018-0491-6 (Sept. 2018).

28. Braun-Munzinger, P., Redlich, K. & Stachel, J. in *Quark–Gluon Plasma 3* 491–599 (WORLD SCIENTIFIC, Jan. 2004). https://doi.org/10.1142%2F9789812795533_0008.

29. Steinbrecher, P. The QCD crossover at zero and non-zero baryon densities from Lattice QCD. *Nuclear Physics A* **982,** 847–850. https://doi.org/10.1016%2Fj.nuclphysa.2018.08.025 (Feb. 2019).

30. Stachel, J., Andronic, A., Braun-Munzinger, P. & Redlich, K. Confronting LHC data with the statistical hadronization model. *J. Phys. Conf. Ser.* **509** (eds Evans, D., Hands, S., Lietava, R., Romita, R. & Villalobos Baillie, O.) 012019. arXiv: 1311.4662 [nucl-th] (2014).

31. Andronic, A. *et al.* The thermal proton yield anomaly in Pb-Pb collisions at the LHC and its resolution. *Phys. Lett. B* **792,** 304–309. arXiv: 1808.03102 [hep-ph] (2019).

32. Braun-Munzinger, P. & Stachel, J. (Non)thermal aspects of charmonium production and a new look at J / psi suppression. *Phys. Lett. B* **490,** 196–202. arXiv: nucl-th/0007059 (2000).

33. Braun-Munzinger, P. & Stachel, J. The quest for the quark-gluon plasma. *Nature* **448,** 302–309 (2007).

34. Matsui, T. & Satz, H. J/ψ Suppression by Quark-Gluon Plasma Formation. *Phys. Lett. B* **178,** 416–422 (1986).

35. Andronic, A., Braun-Munzinger, P., Köhler, M. K., Redlich, K. & Stachel, J. Transverse momentum distributions of charmonium states with the statistical hadronization model. *Phys. Lett. B* **797,** 134836. arXiv: 1901.09200 [nucl-th] (2019).

36. Kirchner, A. private communication.

37. Acharya, S. *et al.* Production of charged pions, kaons, and (anti-)protons in Pb-Pb and inelastic *pp* collisions at $\sqrt{s_{NN}} = 5.02$ TeV. *Phys. Rev. C* **101,** 044907. arXiv: 1910.07678 [nucl-ex] (2020).

38. Abelev, B. *et al.* Pion, Kaon, and Proton Production in Central Pb-Pb Collisions at $\sqrt{s_{\mathrm{NN}}}$=2.76 TeV. *Phys. Rev. Lett.* **109,** 252301. https://link.aps.org/doi/10.1103/PhysRevLett.109.252301 (25 Dec. 2012).

39. Andronic, A., Braun-Munzinger, P., Redlich, K. & Stachel, J. The thermal model on the verge of the ultimate test: particle production in Pb–Pb collisions at the LHC. *Journal of Physics G: Nuclear and Particle Physics* **38,** 124081. https://doi.org/10.1088/0954-3899/38/12/124081 (Nov. 2011).

40. Kreis, L. private communication.

41. Simon-Gillo, J. Low pT phenomena observed in high energy nuclear collisions. *Nuclear Physics A* **566,** 175–182. ISSN: 0375-9474. https://www.sciencedirect.com/science/article/pii/037594749490622X (1994).

42. Csorgo, T. Rapidity dependent low p(t) enhancement. arXiv: hep-ph/9412323 (Dec. 1994).

43. Barrette, J. *et al.* Measurement of pion enhancement at low transverse momentum and of the Delta resonance abundance in Si-nucleus collisions at AGS energy. *Physics Letters B* **351,** 93–98. https://doi.org/10.1016/0370-2693%2895%2900329-j (May 1995).

44. Begun, V., Florkowski, W. & Rybczynski, M. Explanation of hadron transverse-momentum spectra in heavy-ion collisions at $\sqrt{s_{NN}} = 2.76$ TeV within chemical non-equilibrium statistical hadronization model. *Phys. Rev. C* **90,** 014906. arXiv: 1312.1487 [nucl-th] (2014).

45. Abelev, B. *et al.* Centrality dependence of π, K, p production in Pb-Pb collisions at $\sqrt{s_{NN}} = 2.76$ TeV. *Phys. Rev. C* **88,** 044910. arXiv: 1303.0737 [hep-ex] (2013).

46. Ryu, S. *et al.* Importance of the Bulk Viscosity of QCD in Ultrarelativistic Heavy-Ion Collisions. *Physical Review Letters* **115.** https://doi.org/10.1103/physrevlett.115.132301 (Sept. 2015).

47. Ryu, S. *et al.* Effects of bulk viscosity and hadronic rescattering in heavy ion collisions at energies available at the BNL Relativistic Heavy Ion Collider and at the CERN Large Hadron Collider. *Phys. Rev. C* **97,** 034910. arXiv: 1704.04216 [nucl-th] (2018).

48. *The physics of the quark-gluon plasma* (eds Sarkar, S., Satz, H. & Sinha, B.) (2010).

49. Andronic, A., Braun-Munzinger, P., Köhler, M., Redlich, K. & Stachel, J. Transverse momentum distributions of charmonium states with the statistical hadronization model. *Physics Letters B* **797,** 134836. ISSN: 0370-2693. https://www.sciencedirect.com/science/article/pii/S0370269319305507 (2019).

50. Andronic, A. private communication.

51. Andronic, A. *et al.* The multiple-charm hierarchy in the statistical hadronization model. *JHEP* **07,** 035. arXiv: 2104.12754 [hep-ph] (2021).

52. Völkl, M. A. private communication.

Acknowledgment

I would like to thank Dr. Martin Völkl for helping and guiding me through this project, being almost always available for questions and ideas concerning the project. I am very grateful that I could write this thesis under the supervision of Prof. Dr. Johanna Stachel and I would like to thank Prof. Dr. Klaus Reygers for being the second corrector of my thesis. I enjoyed the work on this particularly interesting topic and the time in the ALICE working group at PI. Moreover, a special thanks is dedicated to Andreas Kirchner for being a constant contact person for FluiduM and for his contributions to the success of the thesis. Many people supported me during the writing of this thesis and I would like to express my gratitude to all those people. This is especially dedicated to everyone who proofread parts of the thesis and, of course, my friends and family for their constant support.

Erklärung

Ich versichere, dass ich diese Arbeit selbstständig verfasst und keine anderen als die angegebenen Quellen und Hilfsmittel benutzt habe.

Heidelberg, den ...,